Collisions induced by 11 MeV/nucleon $^{58}Ni + ^{24}Mg$

D. Shapira, J. Gomez del Campo, and M. Korolija*
Oak Ridge National Laboratory, Oak Ridge, Tennessee 37831

J. Shea and C. F. Maguire
Physics Department, Vanderbilt University, Nashville, Tennessee

E. Chavez-Lomeli
Instituto di Fisica, UNAM, Mexico City, Mexico
(Received 7 February 1996; revised manuscript received 15 July 1996)

Measurements of energy spectra for protons, deuterons, tritons, and α particles in coincidence with heavy evaporation residues were made with a large logarithmic detector array which covered the angular range of 3° to 24°. We performed detailed comparisons with statistical calculations which model the evaporative decay of a compound nucleus formed in the collisions. We found out that it was possible to account for the observed energy spectra of the light particles and their relative yields if one assumes initial evaporation from a highly deformed composite system (dinuclear) which at a later stage in the cascade relaxes into a normal compound nucleus. [S0556-2813(97)01705-6]

PACS number(s): 25.70.Jj, 24.60.Dr, 25.70.Gh

I. INTRODUCTION

Nuclear reactions between heavy ions can be used to study nuclear matter populated at extreme states of density, temperature, angular momentum, and composition. To study nuclear matter at such extreme states requires a thorough understanding of nuclear collisions, especially violent collisions involving substantial rearrangement of nuclear matter. Nucleus-nucleus fusion has been studied in nuclear collisions starting at energies below the Coulomb barrier up to bombarding energies well above 10 MeV/nucleon and our understanding of this process has increased during the last few decades, but there remain many outstanding questions. At low energies, below the nucleus-nucleus Coulomb barrier, resonances appear in the composite system formed in collisions between light nuclei [1]. In heavier systems the magnitude of the cross section for fusion, at subbarrier energies, shows a huge departure from predictions based on one-dimensional barrier penetration models and also large variation from one system to another [2]. At higher bombarding energies, the saturation of fusion cross sections in collisions between light nuclei is still not fully explained [3], and the emission of light particles from hot compound nuclei with kinetic energies well below the separation barrier [4] has emerged as a more recent puzzle.

At bombarding energies exceeding 10 MeV/nucleon, processes other than complete fusion become important, and the interpretation of reaction data becomes increasingly complicated. Exclusive studies of particle production in nuclear reactions at these energies mandate the use of large arrays of particle detectors. The work reported here was performed with a large detector array for charged particles, Heavy Ion–Light Ion (HILI) detector [5].

This report concentrates on studies of light particles emitted in reactions between $^{58}Ni + ^{24}Mg$ in coincidence with heavy evaporation residues. Many recent studies that report on the anomaly in the energy spectra of light particles emitted from heavy ion induced reactions (low emission energies) rely on a variety of arguments in assigning the hot compound nucleus as a sole source. Wide angle angular correlations between light particles have served to tag compound nucleus evaporation products [6]. Coincidences with fragments identified as one of two fusion-fission products have also been used [7], as well as in [8,9]. Another technique involves tagging with evaporation residues in coincidence using TOF for isolating all the residues [10] and by identifying low lying gamma transitions in specific evaporation residue channels [11]. For the combination of nuclei and energies studied here it is expected that the primary decay mode of the compound nucleus is light particle evaporation. Therefore, a study of evaporation residues in coincidence with light particles helps to isolate yields of light particles emitted from the composite system. We shall show that the identification of the residues and measurement of their energy spectra provide for efficient and reliable tagging for this process.

The following section provides pertinent details of the experiment. This is followed by a detailed comparison of the data to predictions of the statistical model of compound nucleus decay which is most appropriate for the description of evaporative decay following complete fusion. Discussion of these results, comparison with results from similar studies, and studies of light particle heavy residue correlation are presented in the fourth section. Our conclusions are followed by a couple of appendices which provide some details on experimental techniques and simulations.

II. THE EXPERIMENT

In the experiment a 190 $\mu g/cm^2$ ^{24}Mg (98% enriched) target was bombarded by 630 MeV ^{58}Ni extracted from the

*Present address: Ruder Boscovic Institute, Zagreb, Croatia.

HHIRF coupled accelerators and charged particles from the reaction were detected with the HILI detector array [5]. The HILI (Heavy Ion-Light Ion) detector consists of four large-volume gas filled counters ($20\times15\times30$ cm^3) which provide timing, total energy, energy loss, and two orthogonal position signals (X,Y) for incident heavy ions starting at a threshold energy of approximately $0.1\times Z^2$ MeV up to the highest energy at which the ions are stopped within the gas volume of the detectors. In this experiment full momentum transfer imparts fast forward motion to the composite system and the gas filled ionization chambers are almost transparent to the energetic light particles emitted from this reaction. Behind the gas detector assembly is an array of 192 plastic scintillation ΔE-E detectors in a ''phoswich'' arrangement [12]. These scintillation detectors provide both energy and energy-loss signals for light particles from a threshold energy near $7.0\times Z^2$ MeV (for energy-loss identification) up to a maximum proton energy of 150 MeV. The detector system covers an angular range from 3° to 24° around the beam axis, and is capable of the simultaneous detection of heavy and light ions even when they move in the same direction. The nuclear charge of the heavy fragments is determined by energy and energy-loss measurements (Appendix A shows an example of the detector's performance and methods used to enhance its resolving power). For each of the 192 elements of the light particle hodoscope the thin front layer of the fast plastic scintillator provides both energy loss (ΔE) and timing signals which are used in charge and mass identification.

The beam current in the experiment (typically a few charge nA) was integrated by a shielded Faraday cup placed down stream. The cyclotron rf timing signal was monitored throughout the experiment by accumulating time spectra triggered from a fast scintillation detector positioned close to the target with rf providing the stop time. The time spread throughout the experiment was kept slightly below 1 ns FWHM and enabled easy separation of hydrogen and helium isotopes in every one of the hodoscope elements. The signal conditioning hardware and software as well as the detector system's performance characteristics are described in detail in [5,13]. The energy calibration of the different parts of the detector was carried out using the procedures described in Ref. [5]. Since energy calibration and absolute normalization are pivotal to some of the conclusions reported here, Appendix A provides some detail on the energy calibration and cross section normalization procedures. ^{58}Ni+^{24}Mg data were acquired and stored event by event with different trigger conditions. Inclusive (singles) data as well as coincidences between a heavy and at least one light fragment were taken. The raw count rate in the hodoscope was more then 1 MHz and about 10 kHz in each quadrant of the ionization chamber. The elastic counts were scaled down by a factor of 10 or 100 (using fast hardware gates on DE and E signals) in order to prevent data acquisition and logging from being swamped by elastic scattering data, while retaining a sample of these data for normalization purposes. With coincidence resolving times near 100 ns and hodoscope single rates as high as 10^6/s the random coincidence rate was below 10%. The results reported here are based on a sample of 1.5 million evaporation-residue–light-particle coincidences accumulated in 30 h of running. Some inclusive data on heavy fragment emission from reactions of the same ^{58}Ni beams with ^{24}Mg and ^{197}Au targets were also acquired and used in the normalization of the data as reported in Appendix A.

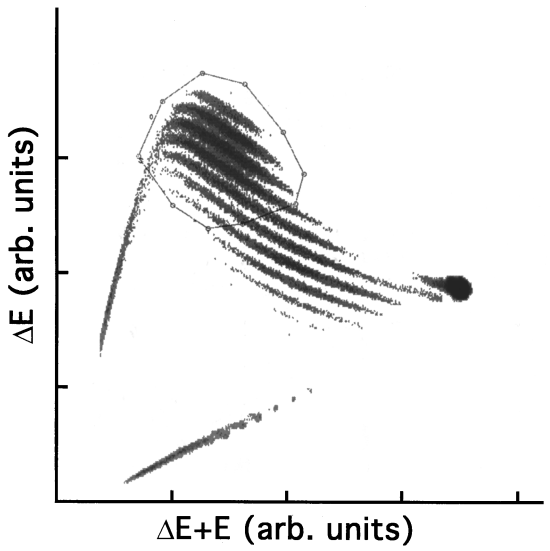

FIG. 1. Energy-loss (ordinate) vs sum energy (abscissa) for ^{58}Ni+^{24}Mg induced reactions.

III. RESULTS

As expected, the four large ionization chambers capture and identify the heavy evaporation-residue-like reaction products quite efficiently. Figure 1 is a two-dimensional map of inclusive data of energy and energy loss measured in the ionization chamber for charged particles from this reaction. The display threshold in this plot was set to a high value so that the evaporation-residue-like yield (outlined in this figure) will be evident. The enclosed region includes products with nuclear charge ranging from $Z=25$ to $Z=34$. This region also contains some products from other processes such as deep inelastic scattering and the heavier partner from asymetric fission channels. In coincidence with these heavy fragments we have also measured light charged particles using the light particle detector array (hodoscope). As a first step we shall examine the data for all heavy ions detected in the gas filled ionization chamber in coincidence with light charged particles. With these data we shall demonstrate that selection of the most heavy fragments ($Z\geqslant30$) and/or events associated with higher light particle multiplicities, can serve to filter out events where full momentum transfer has not occurred.

A. Heavy-fragment–evaporation residues

Figure 2 displays velocity spectra for heavy fragments which are detected in coincidence with one charged particle in the hodoscope. In this figure we show the measured velocity spectra (experimental data, shown with full circles) as well as velocity distributions for the same fragments which are generated by a simulation code which is based on the statistical model for complete fusion followed by light particle evaporation [14]. Typical two-dimensional gates used to select different heavy fragments from the experimental data

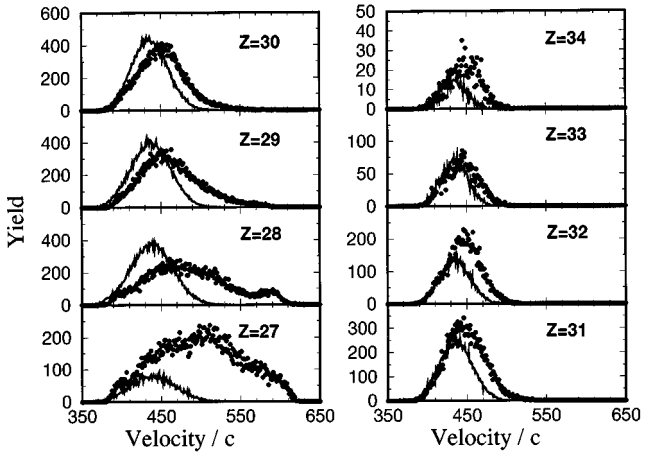

FIG. 2. Velocity spectra (plotted in units of $4096\,v/c$) of heavy fragments from ^{58}Ni+^{24}Mg reactions in coincidence with one light particle hitting the scintillation detector array. Data (circles) and simulation based on statistical model calculations are shown.

are shown in Fig. 15(b). The heavy fragments and the light evaporated particles generated in the statistical simulation are passed through a filter representing the HILI detector. The filter includes the geometric constraints as well as the response of each part of the detector. All comparisons between the model's predictions and our data are made in a similar fashion (see Appendix B for details). As can be seen from Fig. 2, the measured and the model generated spectra have similar kinematic features for particles with $Z \geqslant 30$. The large discrepancies seen for lower masses can be attributed to contributions from other processes (deep inelastic and quasielastic scattering, for example).

One might expect the more central collisions leading to complete fusion to be associated with higher multiplicities of charged particle emission. This is borne out in Fig. 3 which displays the same spectra as shown in Fig. 2 but with the added requirement that more than two charged particles were detected in coincidence with the heavy fragment. We see that when higher multiplicity events are selected the similarity in

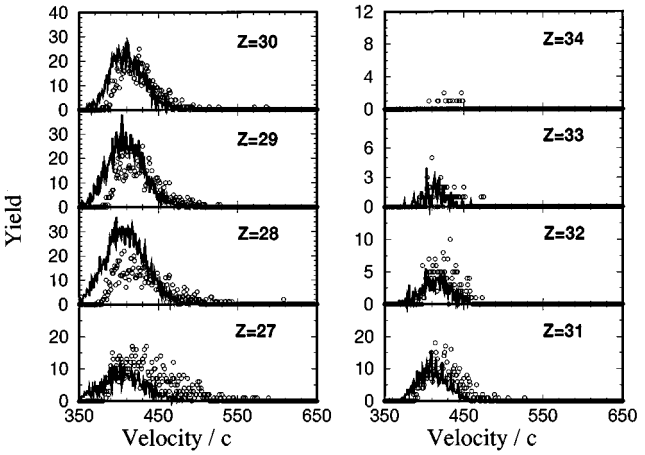

FIG. 3. Velocity spectra of heavy fragments from ^{58}Ni+^{24}Mg reactions. Same as Fig. 2 but with more than two hits in the light particle detector array. Data (circles) and simulation based on statistical model calculations are shown.

shape of the data and the model-generated spectra extends down to $Z=27$. Close examination of Figs. 2 and 3 reveals that even for products with $Z \geqslant 30$, the centroids of the measured velocity distributions, although similar, are somewhat higher ($\sim$2%) than the ones predicted by the statistical model simulations. These small differences could be due to contributions from other processes which produce the same heavy fragments but are associated with processes in which momentum tansfer was not full but close to it (e.g., incomplete fusion with part of the target nucleus). There are many studies of evaporation residue velocity distributions where the residue velocity was measured directly by using time of flight combined with energy measurements ([15–19]). In many cases such measurements allow one to cull out the contribution of different processes which have close to full momentum transfer by using the shape of the fragment's velocity spectra (e.g., [20–22] and others). Our measurements, however, provide only the kinetic energy and the nuclear charge for heavy fragments. The velocities shown in Figs. 2 and 3 are calculated by combining the measured ion energy and an *estimate* of the mass of the fragment. This estimate is obtained by sampling from a mass distribution generated, for each identified charge (Z), by statistical model simulations of the reaction. The uncertainties in our velocity determinations therefore, do not warrant further study of this difference. What Fig. 2 does show is that the measured yields for all fragments with $Z \geqslant 30$ have velocity distribution very similar to those resulting from statistical evaporation decay following complete fusion of projectile and target. Concentrating on these heavier products also serves to exclude light particles that were emitted following fission decay (symmetric or assymetric) of the compound nucleus. We shall therefore base much of the subsequent analysis on light particle yields associated with fragments that have $Z \geqslant 30$.

Before we focus our discussion on these products exclusively we shall examine briefly the light particle spectra associated with *any* charged particle detected in the ionization chamber.

B. Light particles in coincidence with evaporation residues

We now turn our attention to the light particles emitted in this reaction. As noted we first examine spectra of protons and α particles emitted in coincidence with any charged fragment formed in the collision and detected in the gas filled ionization chamber. This selection is bound to incorporate in the spectra light particles emitted from sources other than the hot compound nucleus formed in the collisions. Based on what we saw in Fig. 2 we anticipate, however, that the energy spectra for light particles in coincidence with fragments having $Z \geqslant 30$ are primarily associated with emissions from the compound nucleus. Figures 4 and 5 show the kinetic energies for protons and α particles detected in coincidence with heavy fragments identified by nuclear charge. Note that this yield of light particles is associated with instances in which only one light charged particle registered in the hodoscope in coincidence with a heavy fragment (these correspond to the residue yields shown in Fig. 2). The large experimental yields of protons and alphas associated with $Z=27$ and 28 fragments originate from the emission of these particles following deep inelastic processes in keeping with

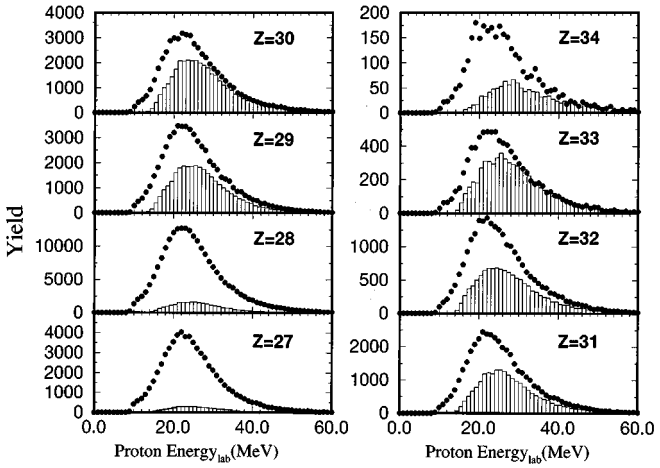

FIG. 4. Energy spectra of protons in coincidence with the indicated fragments and light charged particle multiplicity=1. Circles represent the data and the simualtions appear in histogram form.

the observed yield seen in Fig. 2. It is obvious, then, that any comparison of these particle spectra with those generated by models where the formation of a compoundlike nucleus is postulated becomes meaningful only for those particles in coincidence with fragments having $Z \geqslant 30$. Future comparisons will be made for this subset of data only, with no additional requirement on associated light particle multiplicity (i.e., cpm$\geqslant$1 requirement).

IV. DISCUSSION

A. Energy spectra of light particles

In studying light particle evaporation decay of the hot compound nucleus, statistical evaporation models should provide an adequate description of the data. We therefore use the predictions of a Monte Carlo calculation based on a statistical model that describes light particle evaporation from the hot compound nucleus [14] as a benchmark for quantitative comparison to the data. In our calculation we used standard parameters to calculate the transmission coefficients [23] for light particles emitted in the cascade. The angular momentum cutoff used in the calculation was $J=54\hbar$ and was dictated by the measured magnitude of the evaporation residue cross section (see Appendix A). A level density parameter of $a=A/10$ was used in most calculations and the dependence of deformation on angular momentum described by Huizenga *et al.* [24] was used. Because of the complexity of the detector, comparison to the data is done after running the model simulations through the constraints of the detector system. The appendices at the end of the article provide some detail on how these ''detector filters'' were constructed, tested, and used. All our comparisons with simulated data shown in this work are generated with the same number of total events and therefore form a basis for comparing yield ratios predicted by the simulation with the experimentally observed ratios. As can be seen the model based on statistical evaporation from a spherical compound nucleus misses much of the observed yields at the lower kinetic energies. A significant fraction of the emitted particles appear to emerge at energies below the Coulomb barrier for emission from the compound nucleus. Both protons and α particles show the same behavior (see Figs. 4 and 5). This is in keeping with previous studies of light particle emission from heavy ion induced reactions (e.g., [6–11]). There were different approaches used to explain this discrepancy: changes in level density parameters at high excitation energy [25,26], large deformation of the compound nucleus [27,28] or no parameter changes at all [29].

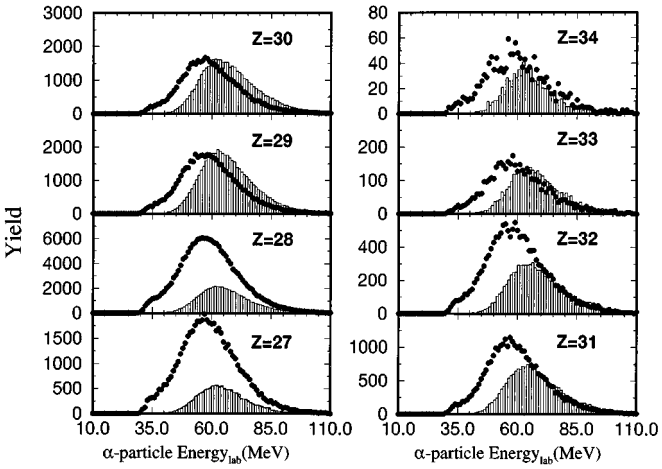

FIG. 5. Energy spectra of α particles in coincidence with the indicated fragments and light charged particle multiplicity=1. Circles represent the data and the simualtions appear in histogram form.

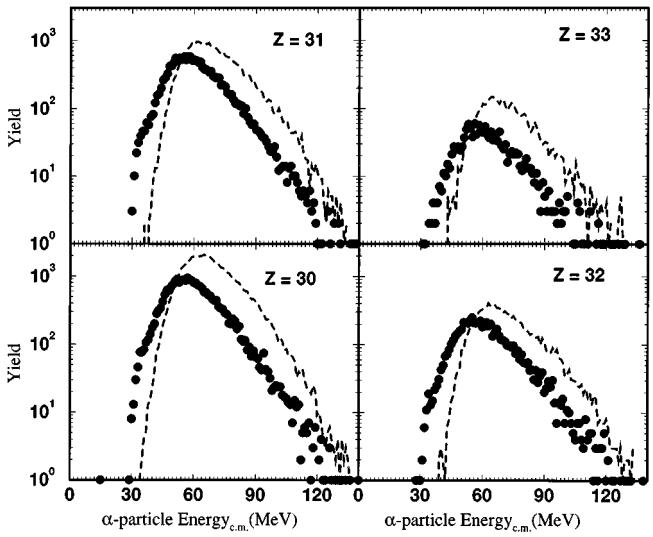

FIG. 6. α particle spectra, comparison of data and statistical model predictions. The velocity spectra of the fragments that are in coinicidence with these particles are shown in Fig. 2. They appear fully damped.

In the following discussion we shall focus our attention on the α particle spectra in coincidence with identified fragments with $Z \geqslant 30$. These spectra, shown in Fig. 6, are associated with residuelike fragments and display the largest discrepancy with statistical model predictions. It is straightforward to associate the excess of α particles emitted at low energy with large deformation of the emitting nuclei. Studies which have addressed this low energy excess account for the deformation by increasing the radius parameter used in the

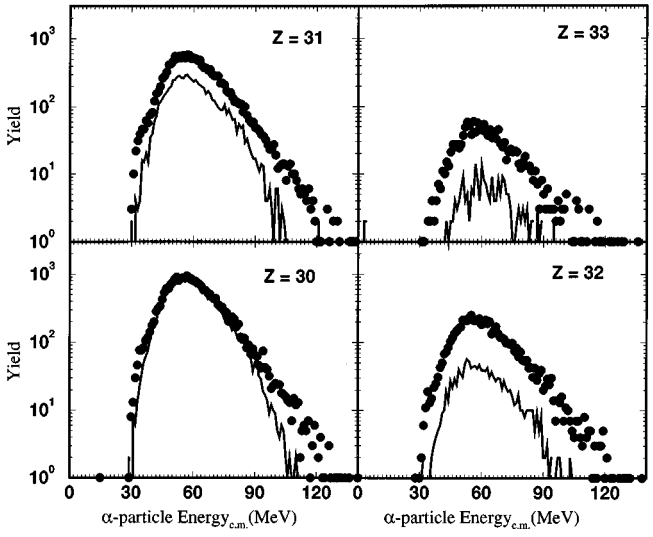

FIG. 7. α particle spectra, comparison of data and statistical model predictions, with large permanent deformation added.

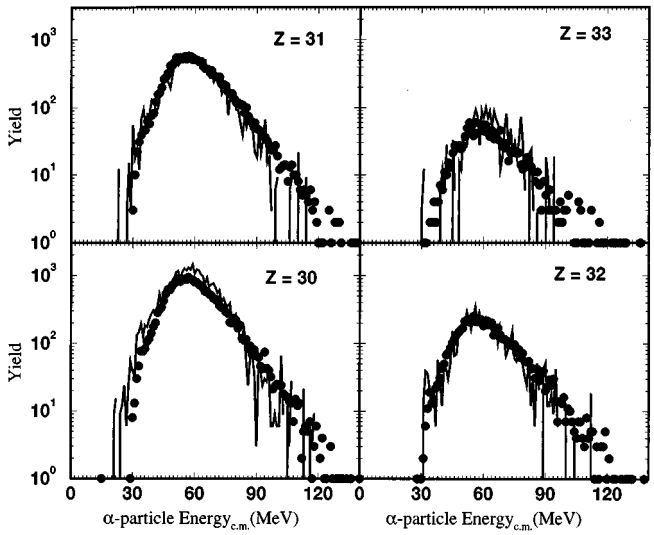

FIG. 8. α particle spectra, comparison of data and predictions from a statistical model with a dinuclear shape included.

level density for all residual nuclei as well as in the optical model parameters used to calculate the penetrabilities for particle emission [27,28]. This is equivalent to assuming large deformation of the hot compound nucleus which persists throughout the cascade. There is no doubt that such a parametrization does lower the emission barriers and could explain the excess in low energy emission of charged particles. We have attempted a similar parametrization, and found that in our calculation we had to use $r_0=2.0$ to account for the low energy yields present in the data. The predicted alpha particle yields in coincidence with different heavy fragments, identified by Z, are compared to the data in Figs. 6 and 7. The same number of Monte Carlo events were used in these and in subsequent plots. It is clear that the cascade in which deformation is frozen throughout results in α particle spectra with the correct energy distribution. It is also apparent that the relative yields of α particles associated with different fragments is skewed toward lighter mass fragments. This is not surprising since the lower kinetic energy of the emitted α particles will result in less energy being removed per emission, which leads to longer cascades. Using a smaller radius parameter will result in better relative yields but the shift in barrier position will not be sufficient. It could well be that the assumption of a deformation that lasts permanently throughout the cascade is unrealistic [8]. It is plausible that early in the cascade the emission times of particles can be very short (10^{-21} s) resulting in these particles being emitted from a very deformed, probably a dinuclear shape. Following one or several emissions, as the excitation energy decreases, particle emission times become long enough to allow for shape changes toward a more spherical nucleus to occur. Shown in Fig. 8 are results of a simulation which allows for such shape changes. The two colliding nuclei first form a fully damped dinuclear system, i.e., the kinetic energy in excess of the barrier is transformed to excitation energy of the two fragments. These excited nuclei are allowed to decay via particle emission and then the system collapses into the normal compound nucleus [30,31]. Figure 8 shows the spectra predicted by this calculation. One can see that the required barrier shift is not accompanied by the lowering of α particle yields associated with heavier fragments. Clearly the desired effect was achieved through the introduction of extreme deformation (dinuclear shape) in the initial stage followed by decay of a compound nucleus wherein moderate deformation is introduced in the usual way using nuclear potentials with standard parameters for the different decay channels and residual nuclei moments of inertia which depend on deformation (spin).

B. Relative yields of light particles

A recent article by Korolija *et al.* [32] addresses a similar problem of particle emission from a composite system undergoing shape changes. They contend that the ratio of emission of more tightly bound to less tightly bound particles in two reactions can provide a measure of the time scale of the shape changes. They performed a comparative study of two reactions leading to the same compound nucleus (Yb). Although we do not have the data suitable for such a comparative study of two reactions leading to the same compound nucleus it is interesting to note that a similar trend can be seen in our data. Figures 9–11 present the yield ratios for proton/deuteron, α/triton, and proton/triton emissions in this reaction. The light particle yields were taken in coincidence with heavy residuelike fragments having $Z \geqslant 30$, thus ensuring that the particle yields integrated are primarily associated with evaporation residuelike yields. In theses figures we compare the experimental ratios to the predictions of the statistical model, i.e., evaportation following complete fusion of target and projectile. It is obvious from all three figures that the number of deuterons and tritons (''expensive,'' energywise) relative to proton and α's emitted are well below statistical model predictions although all light particles are associated with evaporation residuelike fragments. Included in these figures are also the ratios predicted by the two other calculations. One calculation was for the emission from an extremely deformed compound nucleus, with the same parameters as the one shown in Fig. 7. The third (dashed) curve shows the results from the calculation involving emission from an early dinuclear stage followed by the cascade from

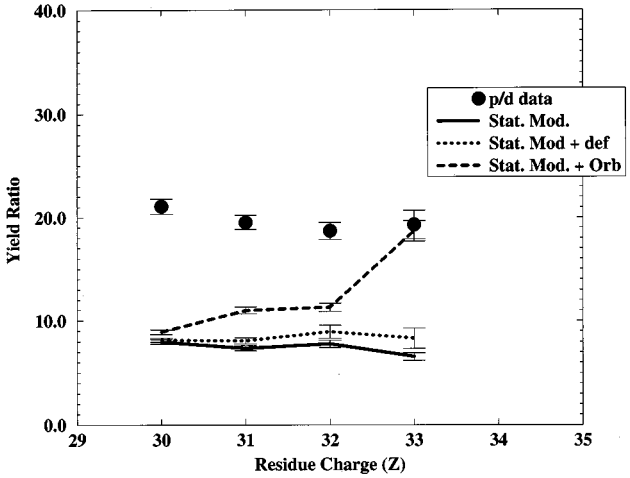

FIG. 9. Ratio of proton to deuteron yield in coincidence with heavy fragments having $30 \leqslant Z \leqslant 33$. Three different simulations are shown and the parameters used are described in the text.

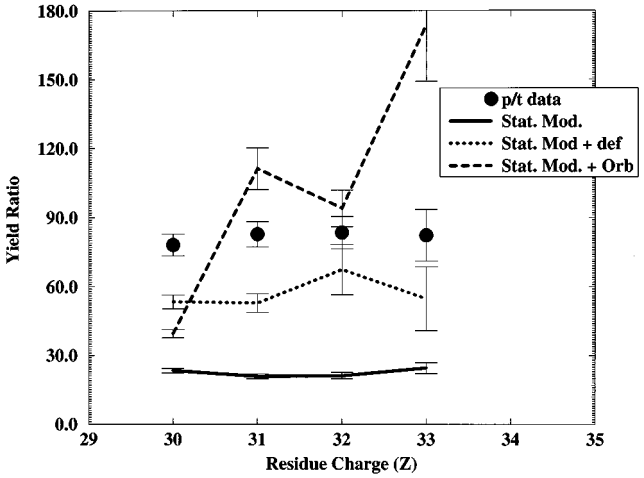

FIG. 11. Ratio of proton to triton yield in coincidence with heavy fragments having $30 \leqslant Z \leqslant 33$. Three different simulations are shown and the parameters used are described in the text.

the compound nucleus formed after the first emission stage. Although neither calculation fits the data, and none was intended, it appears that the introduction of initial deformation (or emission from the dinuclear shape) does improve that ratio.

C. Heavy-ion–light-ion angular correlations

From what has been presented so far it appears that the most substantial disagreement with the straightforward statistical model for compound nuclear decay appears in the emission spectra of light particles. The energy spectra of these particles as well as the velocity spectra of the heavy fragments detected in coincidence show that these originate from a fully damped system. If there were dynamic effects that caused the emission of these nucleons at an early stage of the reaction (from a fast moving projectile like or almost stationary target like fragment) these might exhibit themselves through angular distributions and correlations. Emission from projectilelike particles at an early stage, for example, will exhibit an excess of light particles emitted in the direction of the incoming particles (probably somewhat deflected). Excess would, again, be gauged quantitatively in comparison to statistical evaporation model predictions. Similarly, early emission from a targetlike component would result in an excess of light particles emitted at wide angles.

The HILI provides heavy fragment and light particle coincidence data over a wide, almost continuous, range of angles. In Fig. 12 we describe the geometry used for our correlation studies. The light ion angular distributions were calculated for heavy fragment emission localized in small bins of polar and azimuthal angle. The results shown in Figs. 13 and 14 are the correlations summed over all the heavy ion emission angle bins. The light particle distributions are

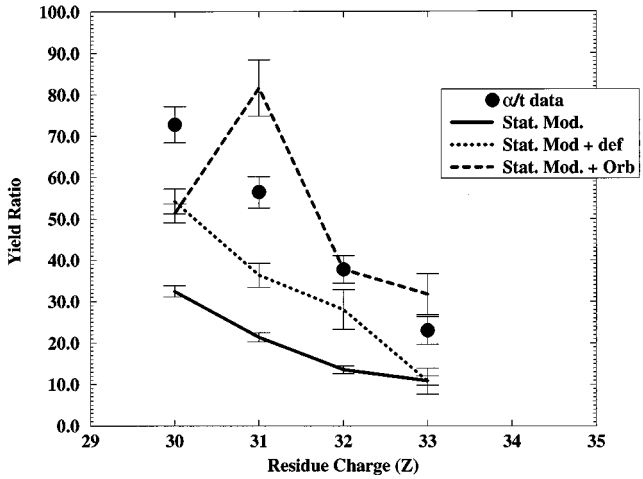

FIG. 10. Ratio of α to triton yield in coincidence with heavy fragments having $30 \leqslant Z \leqslant 33$. Three different simulations are shown and the parameters used are described in the text.

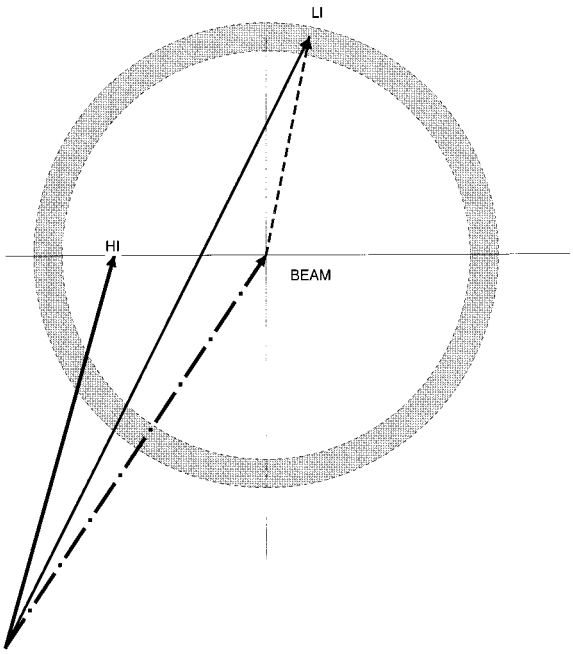

FIG. 12. The geometry used in the correlation studies, the typical ring shown is a 2° wide bin in polar angle of the light ion.

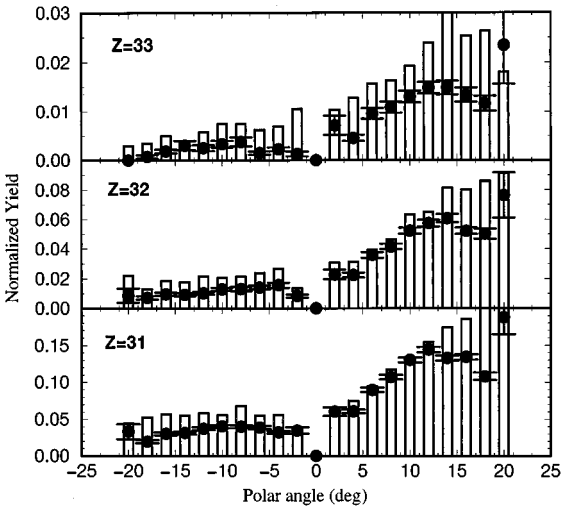

FIG. 13. Angular distibution of protons correlated with heavy residuelike products from ^{58}Ni+ ^{24}Mg reactions. The normalization scheme is detailed in Appendix B and the errors shown originate in counting statistics of the correlation data. The fragments in coincidence with these light particles possess completely damped energy spectra.

summed in 2° bins in polar angle. Light particles emerging on the same side as the heavy fragment are listed as having negative angles. The figures show the experimental correlation data as well as similar correlations calculated with the statistical model of compound nucleus decay. Both correlation data sets were normalized by simulating the acceptance of light and heavy ions with generated pairs of heavy-ion–light-ion coincidences with both particles having a random distribution on a sphere (for details see Appendix B).

The signatures for nonequilibrium emission which we discussed above do not appear in these correlation data. The correlations between light particles and heavy residues (Figs. 13 and 14) show no evidence for emission of light particles from the projectile prior to equilibration (to angles larger than 3°). There is therefore no compelling reason to conclude that dynamic effects associated with emission from the incoming fragments, prior to the attainment of nearly full momentum transfer, plays a role.

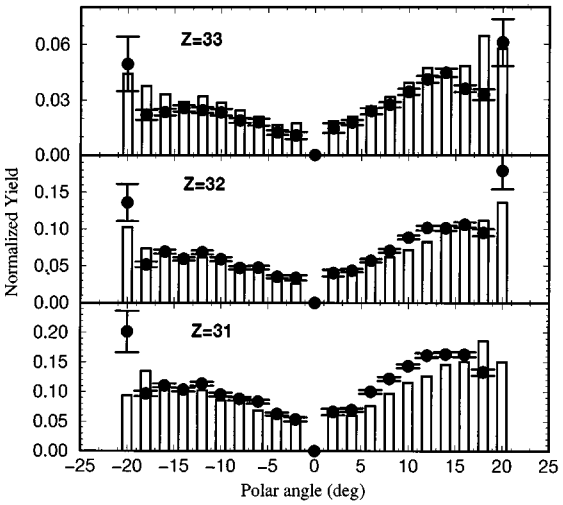

FIG. 14. Angular distibution of α particles correlated with heavy residuelike products from ^{58}Ni+ ^{24}Mg reactions. The normalization scheme is detailed in Appendix B and the errors shown originate in counting statistics of the correlation data.

V. CONCLUSIONS

We have examined coincidences between evaporation residues and light particles from ^{58}Ni+ ^{24}Mg induced collisions. Analysis of correlations between light particles and heavy residues shows no evidence for emission of light particles from the projectile early in the collision. We find, on the other hand, that the statistical model for fusion followed by light particle evaporation misses several features in the data. One needs to account for the low emission barriers of the light particles and the observed light particle yields. We examined in detail the shape of the α particle spectra, the relative yield of α particles associated with different residue charges, and the ratio of α to triton emission.

We were able to account for the low emission barriers as well as the relative yields best by assuming the initial formation of a highly deformed composite system, or alternatively a dinuclear system, composed of the two highly excited incoming nuclei, which later in the cascade revert to a more conventionally shaped compound nucleus.

It would be interesting to perform a similar study on a symmetric system where the expected delay times for shape equilibration should be even longer.

ACKNOWLEDGMENTS

Oak Ridge National Laboratory is managed by Lockheed Martin Energy Research Corp. for the U.S. Department of Energy under Contract No. DE-AC05-96OR22464.

APPENDIX A: ENERGY CALIBRATION AND NORMALIZATION OF HEAVY FRAGMENT DATA

1. Signal enhancement and energy calibration of ionization chamber

The methods and procedures used for calibrating position and energy signals for different components of the HILI detector are described in [5] and were followed here. Additional information and a correction to Fig. 15 in Ref. [5] appear in this appendix.

Figure 15(a) is similar to Fig. 14 in Ref. [5] and shows the two-dimensional spectrum of energy loss versus sum of energy deposited in the ionization chamber, which is used for element identification. The appearance of two strong groups where one quasielastic Ni is expected is puzzling and hampered correct element identification. Subsequently, the dependence of the energy and energy-loss signals from the ionization chamber was examined as a function of the position where the particle entered the detector. The energy-loss signal registered a very strong dependence on the vertical position in the detector. Scattering of Ni from Au was used to establish the kind of dependence seen in Fig. 16. In addition to the overall ''gentle'' dependence on position there is the sharp change seen at position signals near the detector's cathode (edge furthest away from the anode). We have since

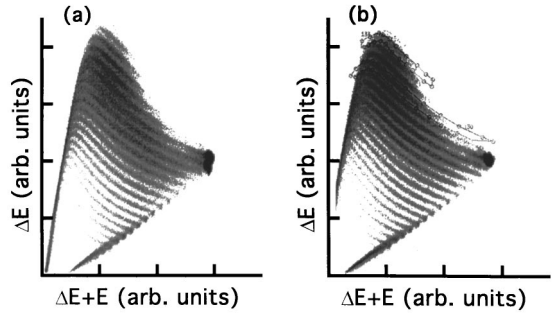

FIG. 15. Energy-loss (ordinate) vs sum energy (abscissa) for ^{58}Ni+^{24}Mg induced reactions (a), (b) is the same after correcting for $\Delta E3$ dependence on the vertical position. Also shown are two gates drawn to select fragments with $Z=30$ and 33.

traced this strong position dependence to the front potential grading foil. This foil was inserted to prevent such position dependence but since it was framed only on three sides sagging along one edge did occur. Once we applied corrections, derived from the Ni+Au elastic data, the same energy vs. energy-loss spectrum for Ni+Mg has improved as shown in Fig. 15(b). Correct identification of the different elements was crucial to our energy calibration. For ions which were not stopped in the detectors one can calculate the maximum energy which they can deposit in the detector and use this value as a fiducial (calibration point). Changes in the assignment of atomic number to these lines resulted in the calibration line displayed in Fig. 17 (which replaces Fig. 15 in Ref. [5]).

2. Normalization procedure: Absolute cross sections

Absolute normalization of the data was done in the usual way, counting the reaction product yield, integrating the beam current, and using target thickness data (targets were made out of rolled Mg foil). Uncertainties in beam integration and target thickness measurements could be substantial, therefore, elastic scattering measurements of ^{58}Ni+^{24}Mg were also used to verify our normalization. To that end singles inclusive data were measured and were used to inte-

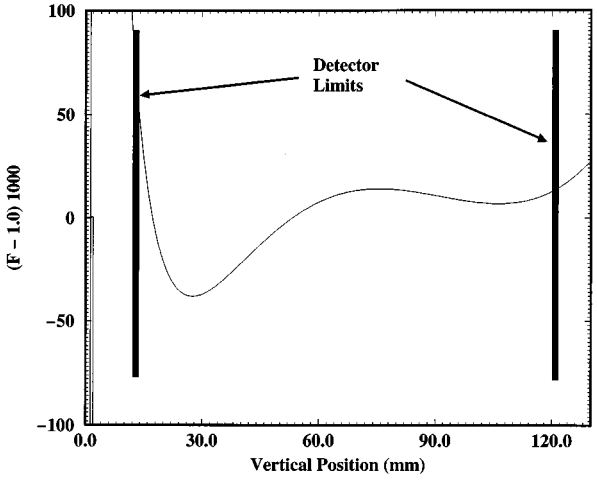

FIG. 16. Energy-loss (abscissa) vs vertical position (ordinate) for ^{58}Ni+^{197}Au scattering.

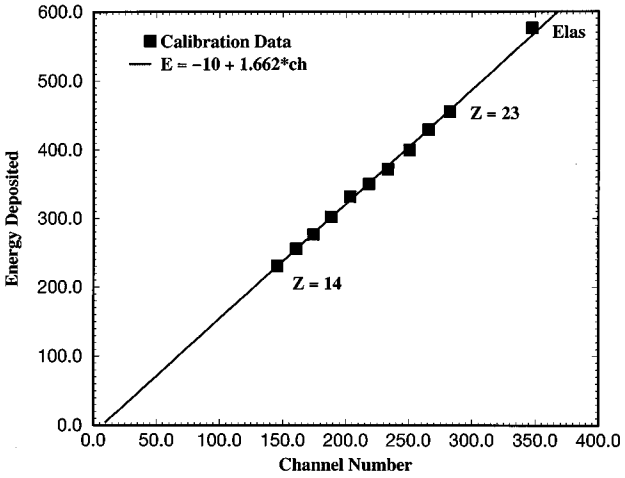

FIG. 17. Energy calibration curve for the ionization chamber.

grate the cross sections for elastic and for fusion-evaporation products. Comparison of elastic data and calculation was done by integrating the data and simulated data (calculation) over concentric, 0.5° wide rings around the beam axis. The simulated (calculated elastic) data were integrated using the detector filter (see Appendix B) and the results were compared to experimental data. Elastic and inelastic scattering to the 2+ states in ^{24}Mg and ^{58}Ni were calculated with the coupled channel code, PTOLEMY [33], using potentials calculated by folding phenomenological nucleon-nucleon effective interactions which were used successfully in studies of heavy ion elastic and inelastic scattering [34].

In a perfect world the ratio of experimental to simulated yield would be 1.0. Figure 18(b) shows substantial variations of that ratio for the angular range 3.5°–8.0° (corresponding to 12°–27.5° in the center of mass). The large variations could be due to our inability to account for elastic scattering in this particular case or some inadequacy of our detector filtering routine. To check the latter we examined some inclusive ^{58}Ni+^{197}Au data taken during the same experiment and the similar ratio of calculated and experimental cross

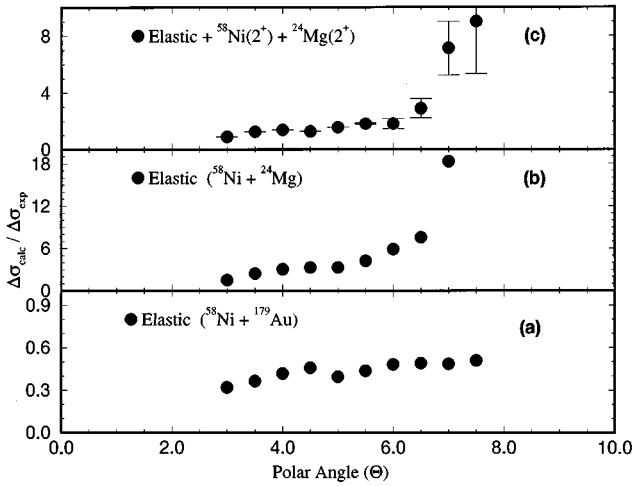

FIG. 18. Ratio of simulated and experimental yields integrated over 0.5° wide rings. The data were taken with 630 MeV ^{58}Ni on Au and Mg targets, the simulations are explained in the text.

sections is shown in Fig. 18(a). The ratio here is fairly constant (it is not close to one because we do not know the Au target thickness). The small deviations from a constant ratio, especially at the most forward angles, can be ascribed to inaccuracy in the filter geometry input. These deviations were also used to correct the elastic scattering simulations for ^{58}Ni+^{24}Mg. It is clear though that these minor corrections will not solve the problem we have in describing the elastic data. The ''elastic'' data here were obtained with $\geqslant$6 MeV resolution in the energy measurement for the detected particle (about 1% in the large ionization chamber). Therefore the data presented as ''elastic scattering'' combine the elastic as well as inelastic scattering yields. We have not attempted to calculate the inelastic scattering to all the states available within 6 MeV from the ground state. At smaller scattering angles however, where more peripheral processes dominate, inclusion of the cross section for the excitation of the lowest 2+ states in the target and projectile results in a near constant ratio of calculated and experimental cross sections. The ratio at angles below 6.5° stays fairly constant with values near 1.2. Subsequently, the evaporation residue cross sections, measured in the same inclusive data runi, were normalized by that factor and the integrated cross section (obtained from integrating the experimental data between 3.0° and 20°) yields an absolute cross section for evaporation residue production in this reaction equal to

$$\sigma = 620 \pm 100 \text{ mb}.$$

The large error is mostly due to the extrapolation of the measured data to angles below 3° which was necessary to obtain an estimate of the total evaporation residue cross section. The main impact of this determination is in the choice of angular momentum cutoff employed in the statistical calculation. This choice of angular momentum cutoff also affects relative quantities such as angular distributions, and the ratio of alpha particle and proton yields in the evaporation process.

APPENDIX B: THE DETECTOR FILTER

1. Inclusive measurements

HILI provides good, almost continuous, coverage for light particles and heavy fragments over a limited angular range. This makes it a useful tool for correlation studies. The extraction of correlation data are however complicated by several factors, among them are finite granularity, especially for light particles, the hodoscope's elements ''integrate'' data over finite (2°) bins; complicated geometry, coverage is compromised by the hardware blocking particle access to the detector's sensitive areas; finally, some of the hodoscope's elements were down during the experiment. Because of the rectangular geometry it is not straightforward to correct for the above-mentioned effects using analytical geometric calculations. To that end we use a HILI detector filter, a program segment which uses as input a data base containing the actual detector dimensions and threshold behavior, as well as the status of each detector (on or off). This filter is used to verify whether particles generated in simulated events do indeed register in the detector. This filter has been used extensively in comparing the measured data with theoretical model predictions.

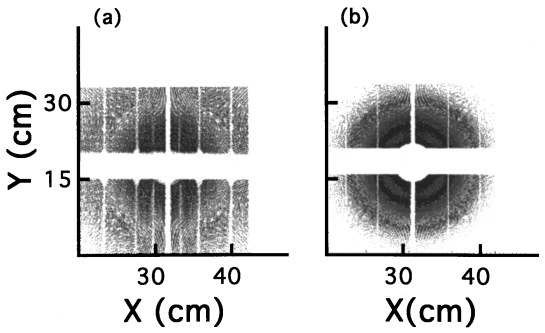

FIG. 19. *X*-*Y* map showing ionization chamber hits for Ni+Mg data (left) and evaporation residues from simulations using statistical model calculations for the same system.

A visual check of the filtering routines appears in the two displays which give us a ''bird's eye view'' of the detected products. A comparison of these *X*-*Y* maps for particles detected in the Ni+Mg experiment and those from a simulated data summary tape (DST) of events generated by a statistical compound nucleus formation and evaporation model are shown in Fig. 19 for the heavy evaporation residues detected in the ionization chamber. Figure 20 provides the same comparison for protons detected in the hodoscope array and the predicted pattern produced by modeling the statistical decay of the compound nucleus formed in the collision.

2. Cross normalization of correlation data

The particular problem of angular correlations is slightly more complex: We want to examine properly normalized correlation data which could lead to intuitive interpretation of the results, independent of a particular model. When we detect a heavy ion and a light particle in coincidence, the geometric acceptance and efficiency for the detection of both products must be folded in. We ran a simulation where the ''data'' generated were emitted with random polar and azimuthal angular distribution. Each event had one heavy ion and one light particle. These simulations were then passed through the detector filter and the counts were binned into polar angle bins. The resulting counts in each bin provide the relative efficiency for heavy fragment and light ion coincidence detection for that particular detector configuration. Since the detector geometry is rectangular and there is no

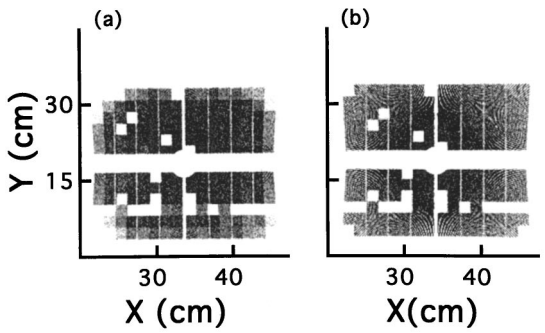

FIG. 20. *X*-*Y* map showing hodoscope hits for Ni+Mg data (left) and light particles from statistical model calculations for the same system.

axial symmetry involved, each detected position of the heavy ion defines a different set of solid angle/efficiency factors associated with these heavy fragment coordinates. Therefore the simulation provides an array of normalization factors for each HI hit, binned by θ and π. For the data presented in this article, 30° in azimuthal (ϕ) and 5° in polar (θ) angle intervals were chosen for binning the sets corresponding to different heavy ion hits.

[1] T. E. Cormier, Annu. Rev. Nucl. Sci. **32**, 271 (1982).

[2] M. Beckerman, Rep. Prog. Phys. **51**, 1047 (1988).

[3] D. G. Kovar, D. F. Geesaman, T. H. Braid, Y. Eisen, W. Henning, T. R. Ophel, M. Paul, K. E. Rehm, S. J. Sanders, P. Sperr, J. P. Schiffer, S. L. Tabor, S. Vigdor, B. Zeidman, and F. W. Prosser, Phys. Rev. C **20**, 1305 (1979).

[4] W. E. Parker, M. Kaplan, D. J. Moses, G. La Rana, D. Logan, R. Lacey, J. M. Alexander, D. M. De Castro Rizzo, P. De Young, R. J. Welberry, and J. T. Boger, Phys. Rev. C **44**, 774 (1991).

[5] D. Shapira, K. Teh, J. Blankenship, B. Burks, L. Foutch, H. J. Kim, M. Korolija, J. M. McConnell, M. Messick, R. Novotny, D. Rentch, J. Shea, and J. P. Wieleczko, Nucl. Instrum. Methods Phys. Res. A **301**, 76 (1991).

[6] R. Lacy, N. N. Ajitanand, J. M. Alexander, D. M. De Castro Rizzo, G. F. Peaslee, L. C. Vaz, M. Kaplan, M. Kildir, G. La Rana, J. D. Moses, W. E. Parker, D. Logan, M. S. Zisman, P. DeYoung, and L. Kowalsky, Phys. Rev. C **37**, 2561 (1988).

[7] R. Lacy, N. N. Ajitanand, J. M. Alexander, D. M. De Castro Rizzo, G. F. Peaslee, L. C. Vaz, M. Kaplan, M. Kildir, G. La Rana, J. D. Moses, W. E. Parker, D. Logan, M. S. Zisman, P. DeYoung, and L. Kowalsky, Phys. Rev. C **37**, 2540 (1988).

[8] J. Boger, J. M. Alexander, R. A. Lacey, and A. Narayanan, Phys. Rev. C **49**, 1587 (1994).

[9] J. Boger, J. M. Alexander, G. Auger, A. Elmaani, S. Kox, R. A. Lacey, A. Narayanan, M. Kaplan, D. J. Moses, M. A. McMahan, P. A. DeYoung, C. J. Gelderloos, and G. Gilfoyle, Phys. Rev. C **49**, 1576 (1994).

[10] G. Nebbia, K. Hagel, D. Fabris, J. B. Natowitz, R. P. Schmidt, B. Sterling, G. Mouchaty, G. Berkowitz, K. Strozewsky, G. Viesti, P. L. Gonthier, R. Wilkins, M. N. Namboodiri, and H. Ho, Phys. Lett. B **176**, 20 (1986).

[11] N. G. Nicolis, D. G. Sarantites, L. A. Adler, F. A. Dilmanian, K. Honkanen, Z. Majka, L. G. Sobotka, Z. Li, T. M. Semkow, J. R. Beene, M. L. Halbert, D. C. Hensley, J. B. Natowitz, R. P. Schmitt, D. Fabris, G. Nebbia, and G. Mouchaty, Phys. Rev. C **41**, 2118 (1990).

[12] M. Bantel *et al.*, Nucl. Instrum. Methods Phys. Res. A **226**, 394 (1981).

[13] K. Teh, D. Shapira, J. W. McConnell, H. Kim, and R. Novotny, IEEE Trans. Nucl. Sci. **35**, 272 (1988).

[14] J. Gomez del Campo and R. G. Stokstad, LILITA A Statistical Evaporation Code, Report No. ORNL/TM7295, 1981.

[15] F. W. Prosser, S. V. Reinert, D. G. Kovar, G. Rosner, G. S. F. Stephans, J. J. Kolata, C. F. Maguire, A. Santo de Toledo, and E. Szanto, Phys. Rev. C **40**, 2600 (1989).

[16] M. F. Vineyard, J. S. Bauer, C. H. Godsin, R. S. Trotter, D. G. Kovar, C. Beck, D. J. Henderson, R. V. F. Janssens, B. D. Wilkins, G. Rosner, P. Chowdhury, H. Ikezoe, W. Kuhn, J. J. Kolata, J. D. Hinnefeld, C. F. Maguire, J. F. Mateja, F. W. Prosser, and G. S. F. Stephans, Phys. Rev. C **41**, 1005 (1990).

[17] G. P. Gilfoyle, M. S. Gordon, R. L. McGrath, G. Auger, J. M. Alexander, D. G. Kovar, M. F. Vineyard, C. Beck, D. J. Henderson, P. A. DeYoung, and D. Kortering, Phys. Rev. C **46**, 265 (1992).

[18] H. C. Britt, B. H. Erkkila, R. H. Stokes, H. H. Gutbrod, F. Plasil, R. L. Ferguson, and M. Blann, Phys. Rev. C **13**, 1483 (1976).

[19] F. Plasil, R. L. Ferguson, H. C. Britt, B. H. Erkkila, P. D. Goldstone, R. H. Stokes, and H. H. Gutbrod, Phys. Rev. C **18**, 2603 (1978).

[20] B. A. Harmon, S. T. Thornton, D. Shapira, J. Gomez del Campo, and M. Beckerman Phys. Rev. C **34**, 552 (1986).

[21] H. Morgenstern, B. Bohne, K. Grabisch, D. G. Kovar, and H. Lehr, Phys. Lett. **113B**, 463 (1982).

[22] H. Morgenstern, W. Bohne, K. Grabisch, H. Lehr, and W. Stoffler, Z. Phys. A **313**, 39 (1983).

[23] C. M. Perey and F. G. Perey, At. Data Nucl. Data Tables **17**, 1 (1976).

[24] J. R. Huizenga, A. N. Bechkami, I. M. Govil, W. U. Schroder, and J. Toke, Phys. Rev. C **40**, 668 (1989).

[25] B. Fornal, G. Prete, G. Nebbia, F. Trotti, G. Viesti, D. Fabris, K. Hagel, and J. B. Natowitz, Phys. Rev. C **37**, 2624 (1988).

[26] B. Fornal, G. Viesti, G. Nebbia, G. Prete, and J. B. Natowitz, Phys. Rev. C **40**, 664 (1989).

[27] R. K. Choudhury, P. L. Gonthier, K. Hagel, M. N. Namboodiri, J. B. Natowitz, L. Adler, S. Simon, S. Kniffen, and G. Berkowitz, Phys. Lett. **143B**, 74 (1984).

[28] Z. Majka, M. E. Branadan, D. Fabris, K. Hagel, A. Menchaca-Rocha, J. B. Natowitz, G. Nebbia, G. Prete, B. Sterling, and G. Viesti, Phys. Rev. C **35**, 2125 (1987).

[29] I. M. Govil, J. R. Huizenga, W. U. Schroder, and J. Toke, Phys. Lett. B **197**, 515 (1987).

[30] J. Gomez del Campo *et al.*, *Proceeding of the XIX Oaxtepec Symposium on Nuclear Physic*, Oaxtepec, Mexico, 1996 [Rev. Mex. Fis. **42**, 101 (1996)].

[31] J. Gomez del Campo, D. Shapira, M. Korolija, H. J. Kim, K. Teh, J. Shea, J. P. Wieleczo, E. Chavez, M. E. Ortiz, A. Dacal, C. Volant, and A. D'Onofrio, Phys. Rev. C **53**, 222 (1996).

[32] M. Korolija, R. J. Charity, N. G. Nicolis, D. G. Sarantites, and L. G. Sobotka, Phys. Rev. C **52**, 3074 (1996).

[33] M. H. Macfarlane and S. C. Pieper, PTOLEMY, a program for heavy-ion direct reaction calculations, Argonne National Laboratory Report ANL-76-11, 1978, unpublished.

[34] G. R. Satchler, Nucl. Phys. **A579**, 241 (1994); G. R. Satchler, private communications.